

Article

Broadband-Transmissive, Frequency-Selective Resorber Design Using Characteristic Mode Analysis

Jie Xiong^{1,2,*}, Baoping Yang^{1,2}, Yanjie Wu¹, Xiongwei Zeng³, Qiuyu Li¹, Rongxin Tang⁴  and Hai Lin^{1,*}

¹ College of Physics Science and Technology, Central China Normal University, Wuhan 430079, China; yangbp@mails.cnu.edu.cn (B.Y.); wuyanjie@mails.cnu.edu.cn (Y.W.); liqiuyu@mails.cnu.edu.cn (Q.L.)

² School of Physics and Telecommunications, Huanggang Normal University, Huanggang 438000, China

³ Wuhan Cigarette Factory, China Tobacco Hubei Industrial Co., Ltd., Wuhan 430032, China; zengxw@wh.hbtobacco.cn

⁴ Institute of Space Science and Technology, Nanchang University, Nanchang 330021, China; rongxint@ncu.edu.cn

* Correspondence: xiongjie82@mails.cnu.edu.cn (J.X.); linhai@mail.cnu.edu.cn (H.L.)

Abstract: This article designs a frequency-selective resorber (FSR) with a broadband transmission window. It is synthesized by a broadband absorber and a frequency-selective surface (FSS). The resistive layer achieves broadband absorption by introducing a tortuous Jerusalem cross load with lumped resistors, and the lossless FSS adopts a three-layer metal structure to realize the broadband transmission window. The absorption mechanism of the resistive layer is analyzed using the theory of characteristic mode. The position of the resistor is determined according to the analysis of mode current distribution and parameter optimization. Prototypes of the structure were fabricated and measured, and the simulation results show that the 1 dB transmission window and the absorption band with $|S_{11}| < -1$ dB are 36.4% and 97%, respectively. Therefore, the designed FSR has potential application prospects in electromagnetic stealth technology and radar cross-section reduction.

Keywords: characteristic modes analysis; broadband transmission; frequency selective resorber; frequency selective surface; radar cross-section



Citation: Xiong, J.; Yang, B.; Wu, Y.; Zeng, X.; Li, Q.; Tang, R.; Lin, H. Broadband-Transmissive, Frequency-Selective Resorber Design Using Characteristic Mode Analysis. *Electronics* **2022**, *11*, 1418. <https://doi.org/10.3390/electronics11091418>

Academic Editors: Antonio Di Bartolomeo and Thomas Walther

Received: 23 March 2022

Accepted: 26 April 2022

Published: 28 April 2022

Publisher's Note: MDPI stays neutral with regard to jurisdictional claims in published maps and institutional affiliations.



Copyright: © 2022 by the authors. Licensee MDPI, Basel, Switzerland. This article is an open access article distributed under the terms and conditions of the Creative Commons Attribution (CC BY) license (<https://creativecommons.org/licenses/by/4.0/>).

1. Introduction

With the development of electromagnetic metamaterials, frequency-selective surfaces (FSSs) have attracted much attention [1–3]. The FSS radomes are capable of reflecting out-of-band energy while ensuring the communication window within the operation band. However, the reflected out-of-band signal can be ineffective for bistatic or multistatic radar cross-section (RCS) reduction. In order to solve this imperfection, a frequency-selective resorber (FSR) with a transmission/absorption window was proposed [4]. FSR is generally used for reducing RCS by absorbing out-of-band energy instead of reflecting it.

In recent decades, some FSRs have been widely proposed and published [5–10]. Existing FSRs can generally be classified into three categories based on the relative positions of the transmission window and absorption bands: (1) the transmission window below an absorption band (TA-FSR) [5,6], (2) the transmission window above the absorption band (AT-FSR) [7,8], and (3) the transmission window within the absorption bands (ATA-FSR) [9,10]. However, in the previous literature, a common feature of FSRs is that they are narrow transmission windows. For some practical applications, for example, the stealth radome of the broadband antenna systems, the broadband transmission property is crucial. The transmission band of the FSR directly affects the radiation performance of the antenna system. There are many methods to achieve the broadband transmission of the FSR [11–19]. For instance, in [11], the researchers achieved a broadband transmission window by using lossless resonators in parallel wave guides with a metal post in the center. In [12], the

broadband transmission is achieved by two layers of patches coupled through an aperture-coupling layer. However, in the above-mentioned literature, the maximum value of the 1 dB transmission band is less than 33.5%. Moreover, ref. [18] adopts an array of the cascaded square patches with two types of modified slot structures in the middle layer to realize three transmission poles to obtain broadband characteristics. Unfortunately, it achieves broadband transmission but does not absorb EM. Some recent work on Jerusalem-cross-based FSS has been published [20–23]. However, it only has narrow pass and stop bands, in addition to the 2D FSR. Several 3D FSRs have been proposed to achieve transmission and absorption [24,25]. In [25], a low-profile 3D FSR with two-sided, wide absorption bands was proposed utilizing a wideband magnetic material and a 3D FSS. However, due to the complexity and higher cost of fabrication, its application is limited.

The equivalent circuit method (ECM) has been widely used to analyze the design of absorption structures [9,16]. However, the ECM has some limitations for complex structures. Some advanced theories in computational electromagnetics can be used to guide the design of absorbing structures. In 1965, Dr. Garbacz first proposed the theory of characteristic mode (TCM) [26]. The TCM is a complete set of orthogonal modes for expanding any induced currents and far-field characteristics due to external sources. With the development of TCM, it has been widely used in various antenna designs [27,28]. Recently, some researchers have begun to use the TCM to analyze the absorbers [29–32].

This paper proposed an FSR with a broadband transmission and low insertion loss (IL). The absorption mechanism of FSR is analyzed utilizing TCM. Moreover, the position and the value of the lumped resistors are decided according to the analysis of the mode current and parameter optimization. The broadband transmission window is achieved by a three-layer metal structure, in which two layers of cascaded square plate resonators are coupled through three rotating C-type apertures in the middle. Finally, the designed FSR has a 1 dB transmission window between 9.3 GHz and 13.45 GHz, corresponding to the FBW of 36.4%, and a one-sided absorption bandwidth of 97%.

2. Theory of Characteristic Mode

The theory of characteristic mode can be utilized to perfect electrical conductors, dielectrics and magnetic materials [30]. In general, there are two important evaluation parameters that are often used to judge whether a certain characteristic mode can be effectively excited in the analysis of eigenmode theory, namely, eigenvalue and mode significance (MS).

(1) Eigenvalue:

According to the TCM, the total distribution of currents is regarded as the modal weighting coefficients (α_n) and the mode current (J_n):

$$\alpha_n = \frac{\langle \vec{E}_i(\vec{r}), \vec{J}_n \rangle}{1 + jJ_n} \quad (1)$$

$$J = \sum_n \alpha_n J_n \quad (2)$$

where λ_n stands for the eigenvalue of mode current (α_n), E_i is called the impressed electric field, and the inner product, $\langle \vec{E}_i(\vec{r}), \vec{J}_n \rangle$, represents the modal excitation coefficient when the external excitation source is coupled with each characteristic mode.

(2) Modal Significance (MS):

MS is an inherent feature of each characteristic mode, to a certain extent. It shows the degree of excitation of each mode in the external excitation sources. The MS can be defined as:

$$MS = \left| \frac{1}{1 + jJ_n} \right| \quad (3)$$

When $MS = 1$, i.e., $|\lambda_n| = 0$, shows that the model can be effective incentive near its resonant frequency. In the actual simulation analysis, $MS > 0.707$ can be considered as the resonant mode.

For the absorption structure, the impressed electric field (E_i) induces mode currents J on the perfect electric conductor (PEC) metallic structure of unit cells. The mode current will motivate a scattered field, which can be analyzed and directed to the design of the absorber by observing the scattered field and mode current. Therefore, we use the TCM to guide the design of the absorption structure.

3. Design and Analysis of the FSR

Figure 1 demonstrates the profile sketch of the proposed FSR. According to the figure, we can conclude that the FSR consists of a resistive layer and a three-layer bandpass FSS structure. The two parts of the structure are separated by air. As shown in Figure 1b, the resistive layer achieves broadband absorption by introducing a tortuous Jerusalem cross, loaded with lumped resistors. Four lumped resistors are loaded to the appropriate location and their resistance value is 150Ω . The resistive layer is printed on a 0.813 mm-thick Rogers 4003C. The relative permittivity and the loss tangent of the dielectric substrate are 3.38 and 0.0027, respectively. As illustrated in Figure 1c,d, the bandpass structural unit is coupled with two layers of cascaded square-plate resonators and three rotating C-type apertures in the middle. The relative permittivity of the bandpass substrate layer is $\epsilon_r = 3$, the loss tangent is $\mu_r = 1$ and the thickness is 2 mm.

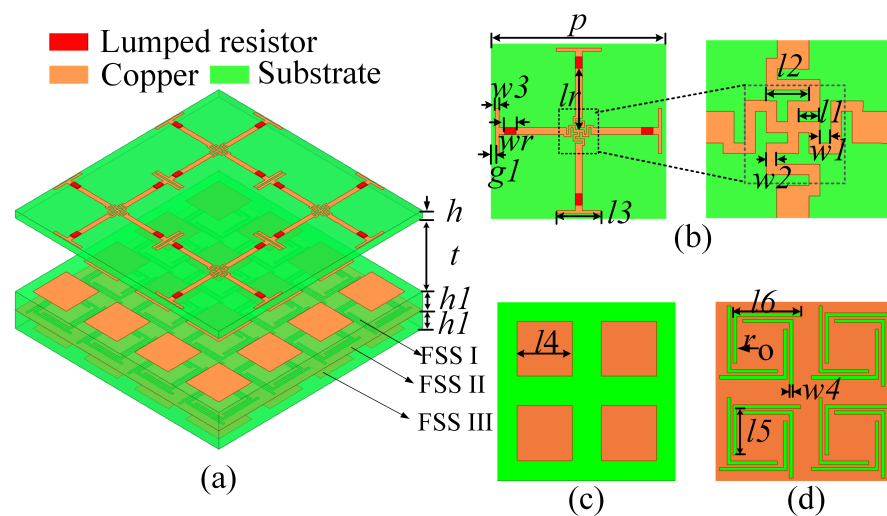


Figure 1. Topology and dimensions of the proposed FSR. (a) Overall FSR diagram. (b) Resistive layer. (c) FSS I and FSS III layer. (d) FSS II layer ($h = 0.813$ mm, $t = 9$ mm, $h1 = 2$ mm, $l1 = 0.4$ mm, $l2 = 0.8$ mm, $l3 = 4.5$ mm, $l4 = 4.7$ mm, $l5 = 3.7$ mm, $l6 = 5.1$ mm, $w1 = 0.2$ mm, $w2 = 0.2$ mm, $w3 = 0.3$ mm, $w4 = 0.3$ mm, $g1 = 0.1$ mm, $l_r = 4.8$ mm, $w_r = 1$ mm, $r = 1.6$ mm).

To investigate the radiating character of the designed FSR from a physical mechanism, the theory of characteristic mode is introduced to analyze the structure of the resistive layer. The radiation patterns and mode currents are simulated by applying moments-based TCM. Figure 2a shows the mode significance (MS) of the tortuous Jerusalem cross. Within 1–16 GHz, there are four modal resonances whose MS are greater than 0.707 at 3.77 GHz, 4.1 GHz, 10.1 GHz, and 12 GHz, respectively. However, since the bandwidths of $MS > 0.707$ are not broad at these frequencies, the top structure only owns a narrow absorption band. Figure 2b shows four modal fields of tortuous Jerusalem cross. It illustrates that, since the main lobes of M1 and M2 are perpendicular to the unit cell, the first mode and the second mode are effective modes under normal incidence. M3 and M4 have weak fields in the Z direction and are not effective modes.

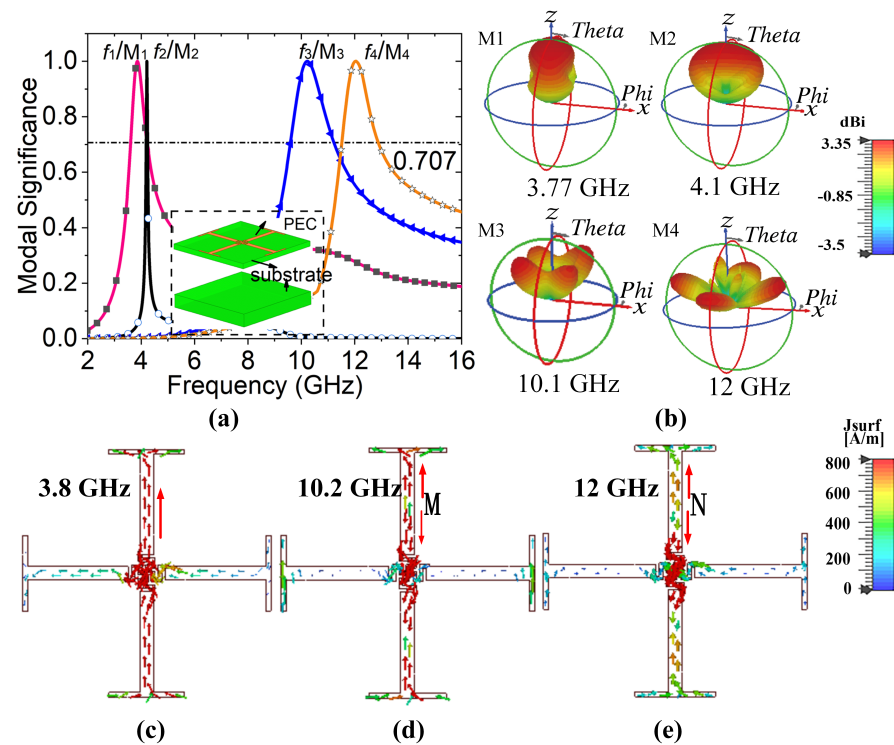


Figure 2. Characteristic mode analysis for the designed absorption structure. (a) Modal significance without R. (b) Modal radiation patterns. (c) Mode current at 3.8 GHz; (d) mode current at 10.2 GHz; (e) mode current at 12.0 GHz.

As shown in Figure 2c–e, we also concentrate on the mode current at the resonant frequencies. At 3.8 GHz, the strong current flows to the top of the Jerusalem intersection along the tortuous line, as shown by the red arrow. Moreover, we analyze the mode current at the frequency points of 10.2 GHz and 12 GHz. It can be observed from Figure 2d,e that the direction of current flow was changed at points M and N. It is shown that the resistive layer structure not only generates strong resonance at three frequency points but also affects different ranges of resonance.

However, the bandwidth of $MS > 0.707$ is narrow. To enlarge the absorption bandwidth, the loss elements (such as lumped resistors) are loaded at metal locations with strong currents. After loading the lumped resistors, the MS of the absorption structure is shown in Figure 3a. It exhibited that the bandwidth of all modes has been broadened. As the resistance increases, the bandwidth will broaden accordingly. It can be seen from Figure 3b that M1 and M2 are effective modes. Therefore, we obtained a bandwidth with $MS > 0.707$ ranging from 1.9 GHz to 7.3 GHz. By observing the mode current distribution, it is obvious that the mode current of the structure is weak and the energy is absorbed by the resistors. Similarly, we analyze the mode current at 10.2 GHz and 12 GHz. Unlike the current distribution at low frequencies, the mode current is still strong when the resistors are added at 10.2 GHz and 12 GHz, as shown in Figure 3d,e. On the other hand, we can also see that the current changes direction at the point N at 12 GHz, while the current does not change at the point M at 10 GHz. It implies that the addition of resistors at 10 GHz has a greater effect than at 12 GHz.

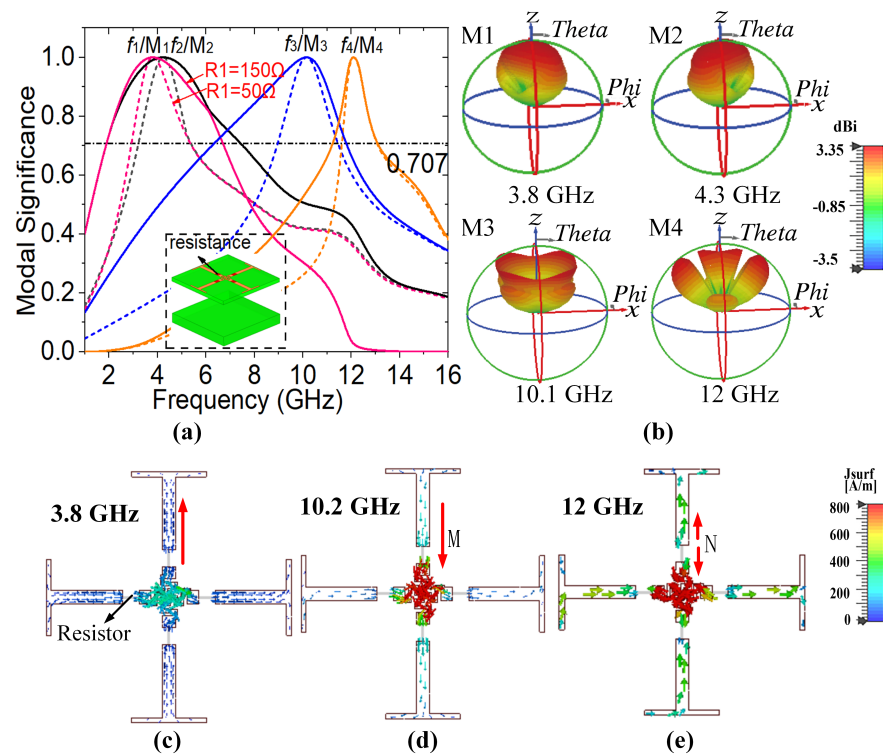


Figure 3. Characteristic mode analysis for the designed absorption structure with R. (a) Modal significance with different R. (b) Modal radiation patterns with R. (c) Mode current at 3.8 GHz; (d) mode current at 10.2 GHz; (e) mode current at 12.0 GHz.

Finally, we obtain the absorption performance shown in Figure 4a. The resistive layer has a good absorption effect in the range of 2.1 GHz–8.0 GHz. Based on the above analysis of characteristic mode and mode current, it is found that the resistive layer resonances at frequency points 10.2 GHz and 12 GHz. In order to better explore the characteristics of these two resonance points, we studied the transmission/reflection coefficient of a resistive layer without a ground layer, as shown in Figure 4b. As observed, the resistive layer has a broadband transmission window ranging from 9.3 GHz to 15.9 GHz. Therefore, we can replace the metal ground in the absorption layer with a transmission structure to realize an FSR with absorption and transmission functions.

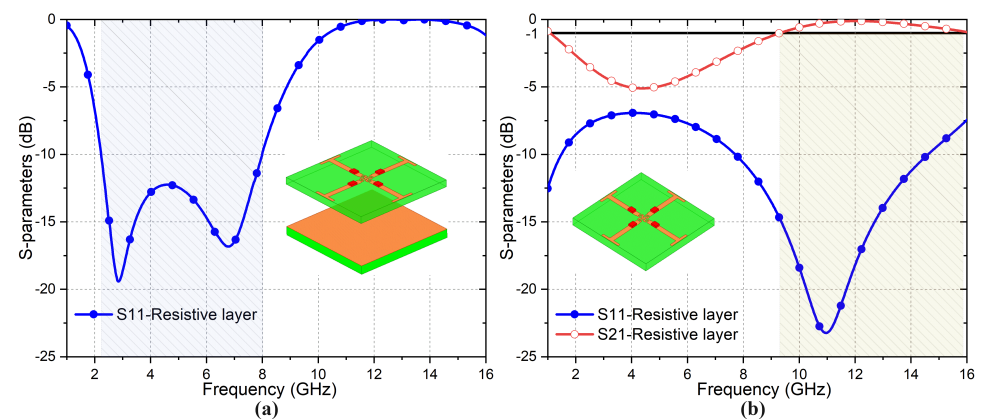


Figure 4. Scattering parameters of resistive layer: (a) absorption performance with a ground plane; (b) transmission/reflection coefficients of resistive layer without a ground plane.

In the bandpass FSS layer, we first designed a single-layer C-slot structure, as given in Figure 5a. It is found that the 1 dB transmission bandwidth of the C-type FSS spans from

11.7 GHz to 13.46 GHz. Then, a cascaded square-patch resonator with an aperture-coupled FSS layer was designed to implement the broadband bandpass FSS. It can be shown that the insertion loss over 7.1–12 GHz is less than 1 dB. To further broaden the passband bandwidth, the C-type structure and the coupled FSS structure are combined into the three-layer FSS. The frequency response of the three-layer FSS is depicted in Figure 5b. As observed, the 1 dB transmission window ranges from 7.56 GHz to 13.46 GHz with the FBW of 56.1%. Obviously, the proposed three-layer FSS structure achieves a wider transmission bandwidth.

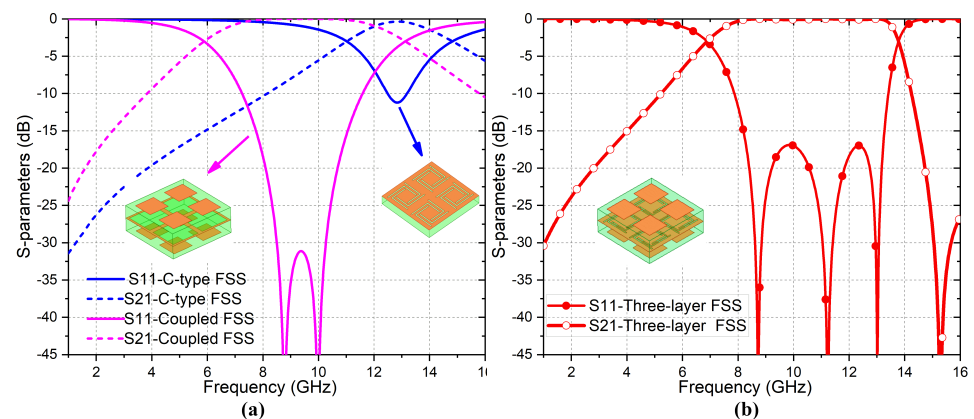


Figure 5. Comparison of transmission characteristics between different FSS. (a) Transmission/reflection coefficients of the C-type FSS and coupled FSS. (b) Transmission/reflection coefficients of the three-layer FSS.

Next, the broadband FSS and resistance layer are integrated to form an FSR with a broadband transmission window, in order to analyze the effects of varied geometric and material parameters on FSR performance. The resistance value (R_1) of the lumped resistor and the position (l_r) of resistors are two key parameters that dominate frequency response performance of the FSR. Figure 6 is given to demonstrate the variation trend of the absorption and transmission performance of the proposed FSR with different l_r and R_1 . As shown in Figure 6a, the IL at the transmission window of the designed FSR is mostly influenced by l_r . According to the previous TCM analysis, the closer the resistance is to the tortuous structure, the better the absorption effect. Unfortunately, the position of the resistors can cause a serious impact on the IL at the passband. As can be seen in Figure 6a, when l_r increases from 1.2 mm to 4.8 mm, the 1 dB transmission window increases from 9.3% to 36.4%. Figure 6b illustrates the absorption efficiency of the proposed FSR is controlled by the value of the lumped resistors. A large or small lumped resistor will lead to poor absorption band performance. After simulation and comparison of several parameters, the absorbing band and 1 dB transmission band are integrated, l_r is 4.8 mm and the resistance R_1 is optimized to be 150 Ω to obtain the best absorption/transmission performance.

Figure 7 shows the frequency response of the proposed FSR for both TE and TM polarizations under different incident angles. The absorption performance of the proposed FSR becomes narrowed with the increase in incident angle under TE polarization, whereas under TM polarization, the absorption performance becomes deteriorated. The reason for this phenomenon is that the impedance of the incident EM is different under various polarizations. As the incident angle increases, the impedance mismatch increases, which leads to the absorption performance of the structure decreasing. Overall, the proposed structure can ensure its angle stability in the case of oblique incidence of 30°. The main reason for the disturbance at passband under two polarization is that the design size of the top structure is too large, so grating lobes are generated at higher frequencies. The disturbance at higher frequency in Figure 7 is mainly caused by the top-layer structure, because the top structure is four times the size of the FSS layer.

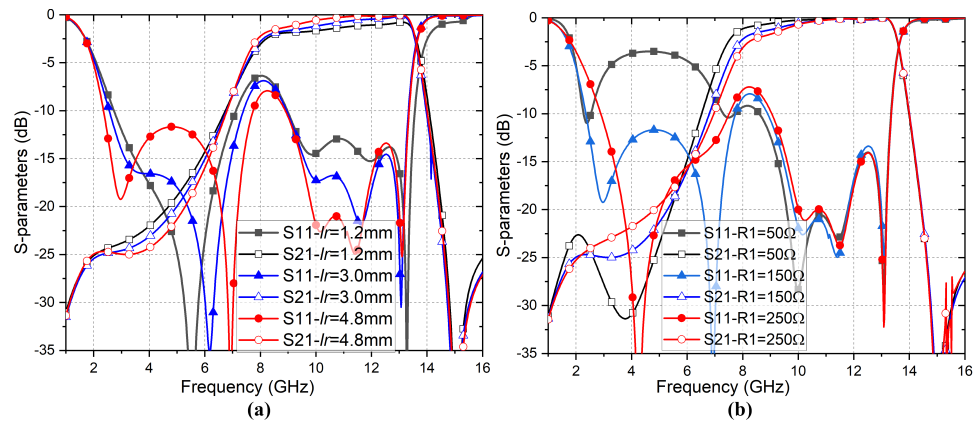


Figure 6. Parameterization optimization of FSR: (a) position of resistors (l_r); (b) lumped resistor (R_1).

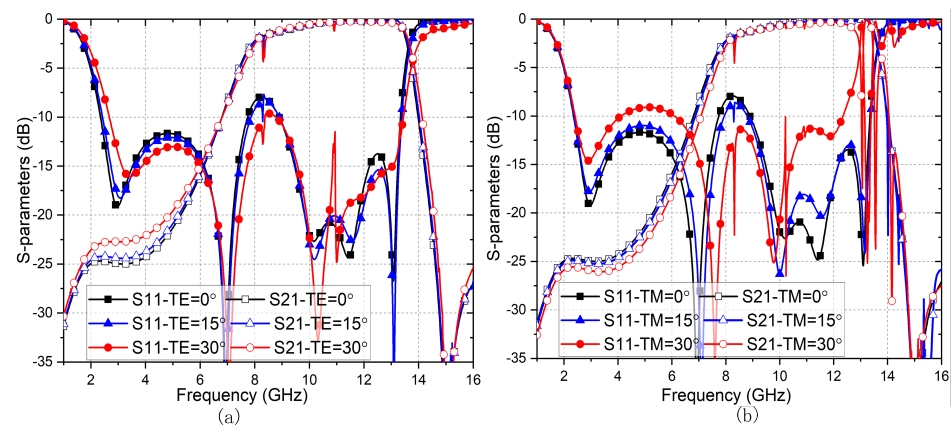


Figure 7. Reflection/transmission coefficients of proposed FSR for oblique incidence under (a) TE polarization and (b) TM polarization.

4. Experimental Verification

To further demonstrate the validity of the reflection and transmission performance of the proposed FSR, a prototype of the proposed FSR was fabricated and measured, as shown in Figure 8. The overall size of the assembled prototype is $300 \times 300 \times 13.8 \text{ mm}^3$ with 20×20 -unit cells. The resistive layers are processed on 0.813 mm-thick Rogers 4003C. For each element, four resistors of 150Ω with 0603 package are welded on Jerusalem structural metal strips. Similarly, for the broadband transmission layer, its periodic pattern of the top layer and the intermediate layer is printed on either side of a 2 mm-thick Teflon substrate, respectively. The bottom patch pattern is processed on another 2 mm-thick substrate. Plastic nylon screws were fixed around the sample to achieve a spacing of 9 mm between the resistive layers and the broadband transmission layers.

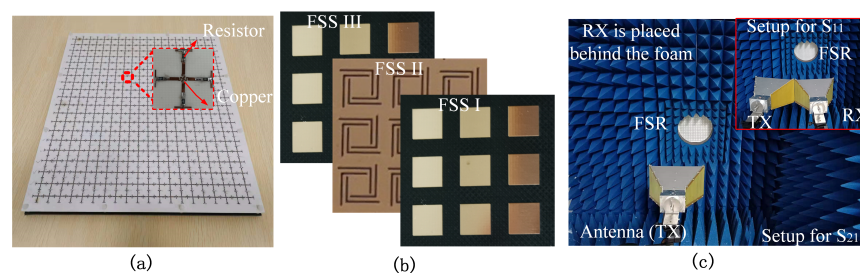


Figure 8. Photograph of the proposed FSR and measurement environment: (a) FSR prototype; (b) metallic patches and rotating aperture; (c) measurement setup.

The reflection and transmission coefficients of the fabricated prototype were measured using the free space measurement method. The setup consists of two standard horn antennas and a network analyzer (Agilent N5230A). Two horn antennas are placed on both sides of the FSR sample when measuring the transmission coefficient, and two horn antennas are side by side toward the FSR sample while measuring the reflection coefficient. Figure 9 shows the measured and simulation results under normal incidence. It is observed that there is a good agreement between the simulation and experimental results. However, there is a slight frequency shift occurring between them, mainly due to unavoidable measurement tolerances and limitations on the electrical dimensions of the prototype.

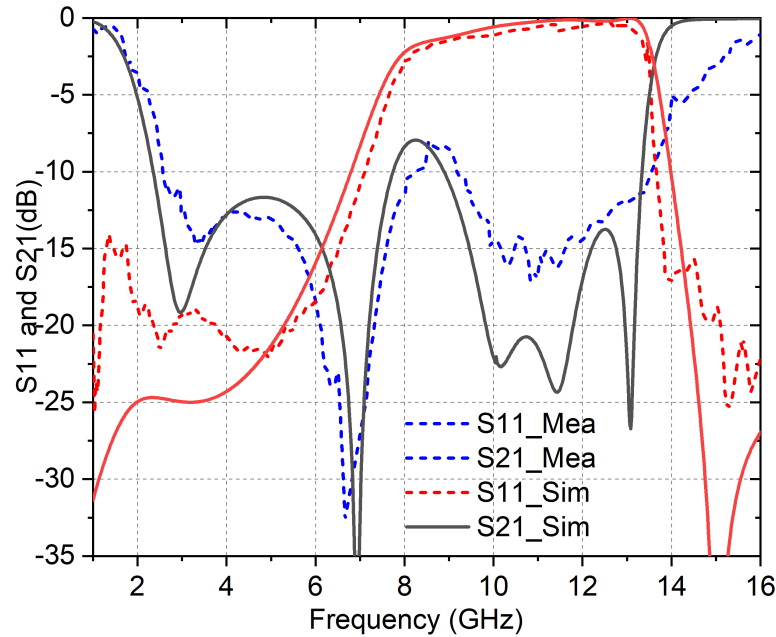


Figure 9. Measured and simulated results of the normal incidence.

To verify the preponderance of the proposed FSR, a performance comparison between our proposed FSR with other published FSRs is tabulated in Table 1. It can be seen from the comparison that the proposed FSR has the advantages in both transmission window and absorption bandwidth.

Table 1. Performance comparison between the proposed FSR and other published FSRs.

Ref.	Transmission (GHz)/FBW	Band	Passband (f_m)/IL	10 dB Absorption (GHz)/FBW	Band	Periodicity
[13]	8.3–11.07/28.6%(1 dB)		N.A. ^a	2.4–7.1/98.9%		$0.096\lambda_L$ ^b
[14]	4.8–7.3/41.3%(3 dB)		6.7/0.31 dB	1.6–4.3/91.5%		$0.16\lambda_L$
[15]	9.0–12.62/33.5%(1 dB)		N.A.	3.88–7.63/65.2%		$0.181\lambda_L$
[16]	4.3–17.4/19.6%(1 dB)		N.A.	3.2–10.7/107.9%		$0.117\lambda_L$
[33]	9.0–12.0/28.5%(1.25 dB)		N.A.	3.18–8.16/87.8%		$0.21\lambda_L$
[34]	3.35–4.86/36.8%(3 dB)		4.25/0.26 dB	2.04–6.2/101%		$0.109\lambda_L$
[35]	9.2–10.0/8.3%(1 dB)		N.A./0.19 dB	5.8–7.8/29.4% 11.8–18/41.6%		$0.19\lambda_L$
ours	9.3–13.45/36.4%(1 dB)		11.3/0.16 dB	2.35–6.78/97.0%		$0.118\lambda_L$

^a the data in the paper is not given; ^b free-space wavelength at lowest working frequency.

5. Conclusions

In this article, we designed and fabricated a frequency-selective rasorber (FSR) with broadband transmission window. The TCM was used to guide the design of the resistive layer with tortuous Jerusalem cross, and the $MS > 0.707$ determines the range of absorption band. The position of the lumped resistor is determined by mode current distribution and parameter optimization. Moreover, the FSS with broadband transmission window is

realized in a high-frequency band by synthesizing the single-layer C-slot structure and the cascaded square patch resonator with hole-coupled FSS layers. The FBW of its 1 dB transmission band and 10 dB absorption window reaches 36.4% and 97%, respectively. At the same time, due to its small periodicity and rotational symmetry, the proposed FSR also exhibits good features under the polarization and incident angles. The proposed FSR can potentially be applied to design stealth radomes for applications from communication to broadband antennas.

Author Contributions: H.L. and J.X. conceived and designed the experiments; B.Y. and Y.W. designed the simulations; Y.W. and Q.L. analyzed the data; X.Z. contributed analysis tools; H.L. and R.T. revised the paper. All authors have read and agreed to the published version of the manuscript.

Funding: This research was funded by the Fundamental Research Funds for the Central University of China under Grant Nos.CCNU20GF004 and CCNU19TS073, the open fund of Guangxi Key Laboratory of Wireless Wideband Communication and Signal Processing under Grant No.GXKL06190202, the open fund of China Ship Development and Design Center under Grant No.XM0120190196 and the National Natural Science Foundation of China under Grant No.41974195. This work is partly supported by the Hongque Innovation Center under Grant HQ202104001.

Data Availability Statement: The data presented in this study are available in article.

Conflicts of Interest: The authors declare no conflict of interest.

References

1. Can, S.; Karakaya, E.U.; Yilmaz, A.E. Design, fabrication, and measurement of textile-based frequency selective surfaces. *Microw. Opt. Technol. Lett.* **2020**, *62*, 3444–3450. [[CrossRef](#)]
2. Fahad, A.K.; Ruan, C.; Nazir, R.; Haq, T.U.; He, W. Dual-Band Ultrathin Meta-Array for Polarization Conversion in Ku/Ka-Band With Broadband Transmission. *IEEE Antennas Wirel. Propag. Lett.* **2020**, *19*, 856–860. [[CrossRef](#)]
3. Omar, A.A.; Kim, J.; Hong, W. A 3-D Lumped-Components-Free Absorptive Frequency-Selective Transmission Structure Featuring Very Wide Two-Sided Absorption Bandwidths. *IEEE Antennas Wirel. Propag. Lett.* **2020**, *19*, 761–765. [[CrossRef](#)]
4. Costa, F.; Monorchio, A. A Frequency Selective Radome With Wideband Absorbing Properties. *IEEE Trans. Antennas Propag.* **2012**, *60*, 2740–2747. [[CrossRef](#)]
5. Bakshi, S.C.; Mitra, D.; Ghosh, S. A Frequency Selective Surface Based Reconfigurable Rasorber With Switchable Transmission/Reflection Band. *IEEE Antennas Wirel. Propag. Lett.* **2019**, *18*, 29–33. [[CrossRef](#)]
6. Sheng, X.; Gao, X.; Liu, N. Design of frequency selective rasorber with high in-band transmission and wideband absorption properties. *IEICE Electron. Express* **2019**, *16*, 20190545. [[CrossRef](#)]
7. Yu, S.; Kou, N.; Ding, Z.; Zhang, Z. Harmonic-Suppressed Frequency Selective Rasorber Using Resistive-Film Sheet and Square-Loops Resonator. *IEEE Antennas Wirel. Propag. Lett.* **2020**, *19*, 292–296. [[CrossRef](#)]
8. Chen, Q.; Guo, M.; Sun, Z.; Sang, D.; Fu, Y. Polarization-independent frequency-selective rasorber with a broadened absorption band. *Aeu Int. J. Electron. Commun.* **2018**, *96*, 178–183. [[CrossRef](#)]
9. Guo, Q.; Su, J.; Li, Z.; Yang, L.Y.; Song, J. Absorptive/Transmissive Frequency Selective Surface With Wide Absorption Band. *IEEE Access* **2019**, *7*, 92314–92321. [[CrossRef](#)]
10. Sharma, A.; Ghosh, S.; Srivastava, K.V. A polarization-insensitive band-notched absorber for Radar Cross Section reduction. *IEEE Antennas Wirel. Propag. Lett.* **2020**, *20*, 259–263. [[CrossRef](#)]
11. Shen, Z.; Jiang, W.; Bo, L. 3-D Frequency Selective Rasorber: Concept, Analysis, and Design. *IEEE Trans. Microw. Theory Tech.* **2016**, *64*, 3087–3096. [[CrossRef](#)]
12. Jin, C.; Lv, Q.; Wang, J.; Li, Y. Capped Dielectric Inserted Perforated Metallic Plate Bandpass Frequency Selective Surface. *IEEE Trans. Antennas Propag.* **2017**, *65*, 7129–7136. [[CrossRef](#)]
13. Chen, Q.; Sang, D.; Guo, M.; Fu, Y. Miniaturized Frequency-Selective Rasorber With a Wide Transmission Band Using Circular Spiral Resonator. *IEEE Trans. Antennas Propag.* **2019**, *67*, 1045–1052. [[CrossRef](#)]
14. Wang, Z.; Fu, J.; Zeng, Q.; Song, M.; Denidni, T.A. Wideband Transmissive Frequency-Selective Absorber. *IEEE Antennas Wirel. Propag. Lett.* **2019**, *18*, 1443–1447. [[CrossRef](#)]
15. Guo, M.; Chen, Q.; Bai, T.; Wei, K.; Fu, Y. Wide Transmission Band Frequency-Selective Rasorber Based on Convolved Resonator. *IEEE Antennas Wirel. Propag. Lett.* **2020**, *19*, 846–850. [[CrossRef](#)]
16. Sheng, X.; Gao, X.; Liu, N. Design of frequency selective rasorber with wide transmission/absorption bands. *J. Phys. D Appl. Phys.* **2020**, *53*, 1–6. [[CrossRef](#)]
17. Yang, Z.; Jiang, W.; Huang, Q.; Hong, T. A 2.5-D Miniaturized Frequency-Selective Rasorber With a Wide High-Transmission Passband. *IEEE Antennas Wirel. Propag. Lett.* **2021**, *20*, 1140–1144. [[CrossRef](#)]
18. Lv, Q.; Jin, C.; Zhang, B.; Mittra, R. Wide-Passband Dual-Polarized Elliptic Frequency Selective Surface. *IEEE Access* **2019**, *7*, 55833–55840. [[CrossRef](#)]

19. Lin, H.; Wu, Y.; Xiong, J.; Zhou, R.; Li, Q.; Tang, R. Dual-polarized bidirectional three-dimensional metamaterial absorber with transmission windows. *Opt. Express* **2021**, *29*, 40770–40780. [[CrossRef](#)]
20. Zahra, H.; Abbas, S.M.; Hashmi, R.M.; Esselle, K.P. Switchable Frequency Selective Surface Based on Composite Flexible Substrate for Modern Communication Systems. In Proceedings of the URSI Asia-Pacific Radio Science Conference (AP-RASC 2019), Delhi, India, 9–15 March 2019; pp. 1–2.
21. Zahra, H.; Abbas, S.M.; Hashmi, R.M.; Matekovits, L.; Esselle, K.P. Bending analysis of switchable frequency selective surface based on flexible composite substrate. In Proceedings of the 2019 IEEE International Symposium on Antennas and Propagation and USNC-URSI Radio Science Meeting, Atlanta, GA, USA, 7–12 July 2019; pp. 2033–2034. [[CrossRef](#)]
22. Zahra, H.; Abbas, S.M.; Shafique, M.F.; Esselle, K.P. A switchable FSS based on modified Jerusalem-cross unit cell with extended top loading. In Proceedings of the 2015 International Symposium on Antennas and Propagation (ISAP), Hobart, TAS, Australia, 9–12 November 2015; pp. 1–2.
23. Zahra, H.; Rafique, S.; Shafique, M.F.; Esselle, K.P. A switchable frequency selective surface based on a modified Jerusalem-cross unit cell. In Proceedings of the 2015 9th European Conference on Antennas and Propagation (EuCAP), Lisbon, Portugal, 13–17 April 2015; pp. 1–2.
24. Omar, A.A.; Huang, H.; Shen, Z. Absorptive frequency-selective reflection/transmission structures: A review and future perspectives. *IEEE Antennas Propag. Mag.* **2019**, *62*, 62–74. [[CrossRef](#)]
25. Wang, Y.; Wang, M.; Shen, Z.; Wu, W. 3-D Single-and Dual-Polarized Frequency-Selective Resorbers With Wide Absorption Bands Based on Stepped Impedance Resonator. *IEEE Access* **2021**, *9*, 22317–22327. [[CrossRef](#)]
26. Garbacz, R.J. Modal expansions for resonance scattering phenomena. *Proc. IEEE* **1965**, *53*, 856–864. [[CrossRef](#)]
27. Lin, F.H.; Chen, Z.N. Low-Profile Wideband Metasurface Antennas Using Characteristic Mode Analysis. *IEEE Trans. Antennas Propag.* **2017**, *65*, 1706–1713. [[CrossRef](#)]
28. Gao, G.; Zhang, R.; Geng, W.; Meng, H.; Hu, B. Characteristic Mode Analysis of a Nonuniform Metasurface Antenna for Wearable Applications. *IEEE Antennas Wirel. Propag. Lett.* **2020**, *19*, 1355–1359. [[CrossRef](#)]
29. Song, Z.; Zhu, J.; Yang, L.; Min, P.; Lin, F.H. Wideband metasurface absorber (metabsorber) using characteristic mode analysis. *Opt. Express* **2021**, *29*, 35387–35399. [[CrossRef](#)]
30. Wu, Y.; Lin, H.; Xiong, J.; Hou, J.; Zhou, R.; Deng, F.; Tang, R. A broadband metamaterial absorber design using characteristic modes analysis. *J. Appl. Phys.* **2021**, *129*, 134902–134928. [[CrossRef](#)]
31. Guo, Q.; Su, J.; Li, Z.; Song, J.; Guan, Y. Miniaturized-Element Frequency-Selective Resorber Design Using Characteristic Modes Analysis. *IEEE Trans. Antennas Propag.* **2020**, *68*, 6683–6694. [[CrossRef](#)]
32. Guo, Q.; Su, J.; Li, Z. Design of circuit analog absorber using characteristic mode analysis. In Proceedings of the 2020 IEEE MTT-S International Microwave Workshop Series on Advanced Materials and Processes for RF and THz Applications (IMWS-AMP), Suzhou, China, 29–31 July 2020; pp. 1–3. [[CrossRef](#)]
33. Jiao, W.H.; Chang, Y.M.; Wang, L.; Wu, W.J. A Dual-Polarized Frequency Selective Resorber with Wide Transmission Band. *Radio Sci.* **2021**, *56*, 7129–7136. [[CrossRef](#)]
34. Xiu, X.; Che, W.; Han, Y.; Yang, W. Low-Profile Dual-Polarization Frequency Selective Resorbers Based on Simple-Structure Lossy Cross-Frame Elements. *IEEE Antennas Wirel. Propag. Lett.* **2018**, 1002–1005. [[CrossRef](#)]
35. Wang, X.; Wang, J.; Yan, M.; Yang, J.; Qu, S. A Frequency Selective Resorber by Engineering Transverse Standing Waves of Surface Current. *IEEE Access* **2021**, *9*, 51703–51709. [[CrossRef](#)]